Transport properties of warm dense neon and krypton at high pressures

Y. J. Gu,[1] W. L. Quan,[2] G. Yang,[3] M. J. Tan,[3] L. Liu,[1] and Q. F. Chen[1,*]

[1]*National Key Laboratory of Shock Wave and Detonation Physics, Institute of Fluid Physics, P.O. Box 919-102, Mianyang, Sichuan, People's Republic of China*

[2]*School of Physics and Telecommunication Engineering, Yulin Normal University, Yulin, Guangxi 537000, People's Republic of China*

[3]*Science and Technology on Space Physics Laboratory, China Academy of Launch Vehicle Technology, Beijing 100076, People's Republic of China*

(Received 17 July 2020; accepted 28 September 2020; published 26 October 2020)

The transport properties of warm dense neon (Ne) and krypton (Kr) are studied by combining self-consistent fluid variational theory (SFVT) with linear response theory (LRT). The components are determined using the SFVT, and the transport parameters, including the electrical conductivity, thermal conductivity, and thermopower, are calculated with the LRT. The relevant scattering mechanisms, including electron-ion, electron-electron, and electron-atom scatterings, are taken into account. An effective potential model in combination with the Muffin-tin model is introduced to further improve the description for electron-atom scattering, which not only includes static, exchange, and polarization interactions but also considers the plasma environmental effects. It is found that for electron-atom scattering, the influence of the plasma density is significant at lower scattering energies but the effects are different for electron-Ne and electron-Kr scattering. For electron-Kr scattering, a plasma density-dependent Ramsauer-Townsend minimum is observed. The obtained transport parameters are compared with the available experiments and other simulations. The plasma phase transition of warm dense Kr is revisited from multiple perspectives based on the numerical simulation results for the electrical conductivity and thermopower. These observations may help one to better understand the transport properties of warm dense noble gases and are an important guide for future experimental designs and theoretical developments.

DOI: 10.1103/PhysRevE.102.043214

I. INTRODUCTION

The high-pressure properties of noble gases under extreme density and temperature conditions play an important role in the evolution and dynamics of planets and stars, especially where they appear in a condensed and purified state. It is crucial to accurately know the transport coefficients, equation of state (EOS), and macroscopic and microscopic physical properties for their constituent materials in the warm dense matter (WDM) regime. High-pressure techniques, such as pulsed power- [1,2], laser- [3,4], two-stage light-gas-gun- [5–7], and explosive-driven facilities [8,9], have been developed and applied to EOS and transport property studies for highly compressed materials. Especially, the pulsed power-driven facility provides a versatile experimental platform for high energy density and inertial confinement science [10]. Various experiments have been performed to measure the EOS and electrical conductivity of warm dense neon (Ne) and krypton (Kr) plasmas [11–14]. Although these experiments present a series of actual electrical conductivities, there are still some discrepancies due to the difficulties of diagnostic equipment under extreme conditions. Different models, including linear response theory (LRT) [15,16], linear mixing rules (LMR) [17], density functional theory (DFT) [18], Lee-More-Desjarlais (LMD) [19], and quantum Langevin molecular dynamics (QLMD) simulations [20], have been applied to study the electrical conductivity of materials at high pressures. These theoretical predictions provide an important reference for the experimental design and optimization of WDM production and diagnostic techniques. However, for LRT and LMR, theoretical predictions of the WDM electrical conductivity require knowledge of the plasma components, the free electron density, and the relevant scattering cross sections; however, it is difficult to calculate the free electron density as there is still no rigorous criterion to divide electrons into free and bound states [21].

Adams *et al.* [15] studied the transport properties of dense noble gas plasmas and calculated their electrical conductivity using LRT. They used the two numerical codes of SAHA IV [22] and COMPTRA04 [23], which were developed for partially ionized plasmas, to provide the required plasma components and the momentum transfer cross sections (MTCSs) for electron-atom scattering based on experimental results and the polarization potential, respectively. The conductivities calculated using the components from COMPTRA04 and the experimental result for the electron-atom cross sections showed good agreement with available experiments for all noble gases up to densities of $\rho \sim 1$ g/cm^3. However, large discrepancies were found between the calculations and experiments above this density. Adams *et al.* [15] described two reasons for these discrepancies. Besides the considerable measurement errors, one is that the species component calculations, especially for heavier elements (Ar, Kr, and Xe), become unreliable for larger densities and for temperatures below $\sim 10^4$ K. The other is that the experimental MTCSs of electron-atom

---

[*] chenqf01@gmail.com

scattering becomes unreliable at higher densities and temperatures because the experiments have only observed isolated scattering events without the effects of a charged surrounding medium. Thus, an accurate picture of the plasma components and electron-atom scattering MTCSs under high densities is crucial for theoretical developments of the WDM transport properties.

In our previous work, a self-consistent fluid variational theory (SFVT) [24] was presented to improve the plasma component calculations for the warm dense noble gases of Ne and Kr. The components were validated as reliable, even at high densities, for Ne beyond 3 g/cm^3 and for Kr up to $\sim$7 g/cm^3 by comparing the EOS between calculations and experiments [24,25], as the EOS calculations strongly depend on the plasma components. Subsequently, we combined the LRT and the SFVT to calculate the components, EOS, and transport coefficients of warm dense Ar [26]. The calculated EOS and electrical conductivities were found to be in good agreement with the available experimental data up to $\sim$4 g/cm^3, showing that the combined SFVT and LRT (SFVT + LRT) is a promising route to study warm dense Ar. In this work, an improved SFVT + LRT is presented to calculate the transport properties of warm dense Ne and Kr to test the applicability of the model as extended into lighter and heavier noble gases. An effective potential model in conjunction with the Muffin-tin model is applied to provide an improved description for electron-atom scattering under warm dense conditions by considering not only the static, exchange, and polarization interactions, but also the effects of the plasma environment. Moreover, the plasma phase transition (PPT) of warm dense Kr is revisited from multiple perspectives using the numerical simulation results of the electrical conductivity and thermopower.

The rest of the paper is organized as follows. The outline of the theoretical method is given in Sec. II. Some results and discussions are presented in Sec. III. Finally, the conclusions are given in Sec. IV.

II. OUTLINE OF THE THEORETICAL METHOD

A. Plasma components in SFVT

The SFVT model is used to calculate the plasma components, which has been described in our previous paper [24]. Here we briefly summarize the main points to calculate the components. Following the SFVT model, at relatively high temperatures and pressures, the possibility of atomic (Kr and Ne) ionization reaction processes is as follows:

$$A^{(k-1)+} \rightleftharpoons A^{k+} + e \;\; (A = \text{Ne or Kr}, \;\; k = 1, 2, \ldots, k_{\max}). \tag{1}$$

The pressure- and temperature-induced ionization reactions result in a multicomponent plasma that consists of atoms, free electrons, and various ion species A^{k+}. The components of such a plasma are governed by the above reactions among the various species. The chemical potentials satisfy the following relations when ionization equilibrium is reached:

$$\mu_k + I_k^{eff} = \mu_{k+1} + \mu_e, \quad k = 0, 1, 2, \ldots, k_{\max}, \tag{2}$$

where I_k^{eff} denotes the effective ionization potential, and μ_k and μ_e are the chemical potentials for A^{k+} and electrons, respectively. Within the SFVT framework, the following SAHA equation, including the particle number density of $n = N/V$, can be derived from the mass action laws together with the condition of ionization equilibrium:

$$\frac{n_{k+1}}{n_k} = \frac{U_{k+1}}{U_k} \exp\left(-\xi - \beta I_k^{eff}\right), \quad k = 0, 1, \ldots, k_{\max}, \tag{3}$$

where $\beta = 1/(k_B T)$ is the inverse temperature, U_k is the internal partition function of A^{k+}, $\xi = \mu_e^{id}/k_B T$ is determined by the Fermi integral $F_n(\xi) = n_e \Lambda_e^3/2$, and $\Lambda_e = (2\pi\hbar^2/m_e k_B T)^{1/2}$ is the thermal de Broglie wavelength for electrons.

To solve Eq. (3), the following equations that represent the conservations of mass and charge, respectively, should be included:

$$\sum_{k=0}^{k_{\max}} n_i = n_H, \tag{4}$$

$$n_e = \sum_{k=0}^{k_{\max}} k n_k, \tag{5}$$

where n_H denotes the number density of heavy particles, which is determined by the formula $n_H = \frac{\rho}{A} N_A$, with ρ as the mass density, A as the atomic weight, and N_A as Avogadro's constant. The components of the plasma can be determined based on Eqs. (3)–(5). The plasma components can be also described by the quantities

$$\alpha_e = n_e \Big/ \left(\sum_{k=0}^{k_{\max}} n_k\right), \quad \alpha_k = n_k \Big/ \left(\sum_{k=0}^{k_{\max}} n_k\right), \tag{6}$$

where α_e is the ionization degree, i.e., the average number of free electrons generated per atom, and k denotes the relative fraction of the ion species A^{k+} with respect to the total number of atoms and ions.

B. Transport coefficients in LRT

1. Brief outline of LRT

The LRT used here is a general approach to determine the transport properties, which was originally developed by Reinholz *et al.* [27], Redmer *et al.* [28], Kuhlbrodt *et al.* [29], and Adams *et al.* [15], following the method of Zubarev [30]. Several calculations have shown that the LRT can be applied over a wide range of densities and temperatures, and from weakly to strongly coupled plasmas. In the LRT framework, the electrical conductivity σ, thermopower κ, and thermal conductivity λ can be given in terms of the Onsager coefficients L_{ik} as

$$\sigma = e^2 L_{11}, \quad \kappa = \frac{1}{eT}\frac{L_{12}}{L_{11}}, \quad \lambda = \frac{1}{T}\left(L_{22} - \frac{L_{12}L_{21}}{L_{11}}\right). \tag{7}$$

The Onsager coefficients are written in the determinant representation within two moment approximations as

$$L_{ij} = -\frac{(-h)^{i+j-2}}{V|D|}\begin{vmatrix} 0 & \frac{j-1}{\beta h}\bar{N}_1 - \bar{N}_0 \\ \frac{i-1}{\beta h}N_1 - N_0 & D \end{vmatrix}, \tag{8}$$

with

$$N_i = \begin{pmatrix} N_{i0} \\ N_{i1} \\ N_{i2} \end{pmatrix}, \quad \bar{N}_i = (N_{0i} \quad N_{1i} \quad N_{2i}),$$
$$D = \begin{pmatrix} d_{00} & d_{01} & d_{02} \\ d_{10} & d_{11} & d_{12} \\ d_{20} & d_{21} & d_{22} \end{pmatrix}, \tag{9}$$

where $h = 5k_BT/2$ is the enthalpy per particle and is the normalization volume of the system. The elements of the vectors N_i and $\bar{N}_i$ represent the generalized particle numbers, i.e., the Kubo products, which are calculated as

$$N_{nm} = N_e \frac{\Gamma(n+m+5/2)}{\Gamma(5/2)} \frac{F_{n+m+1/2}(\beta\mu_e^{id})}{F_{1/2}(\beta\mu_e^{id})}. \tag{10}$$

The elements D in the determinant are the equilibrium force-force correlation functions that can be given as a sum of three parts,

$$d_{ij} = d_{ij}^{ea} + d_{ij}^{ei} + d_{ij}^{ee} \tag{11}$$

and

$$d_{nm}^{ea} = \frac{4Vn_en_a}{3\beta}\sqrt{\frac{2m_e}{\pi\beta}} \int_0^\infty dx x^{n+m+2} e^{-x} Q_T^{ea}(x), \tag{12}$$

$$d_{nm}^{ei} = \frac{4Vn_e}{3\beta}\sqrt{\frac{2m_e}{\pi\beta}} \int_0^\infty dx x^{n+m+2} e^{-x} \left(\sum_j \sqrt{n_j Q_T^{ej}(x)}\right)^2, \tag{13}$$

$$d_{nm}^{ee} = \frac{4Vn_e^2}{3\beta}\sqrt{\frac{m_e}{\pi\beta}} \int_0^\infty dx x^3 R_{nm}(x) Q_T^{ee}(x) e^{-x}, \tag{14}$$

where $R_{n0}(x) = R_{0n}(x) = 0$, $R_{11}(x) = 1$, $R_{21}(x) = R_{12}(x) = 7/2 + x^2$, $R_{22}(x) = 77/4 + 7x^2 + x^4$, and $x = \beta E_k$. The E_k is the collision energy; $Q_T^{ea}(x)$, $Q_T^{ei}(x)$, and $Q_T^{ee}(x)$ are the momentum transfer cross sections (MTCSs) for the electron-atom, electron-ion, and electron-electron scattering, respectively; and n_e, n_a, and n_j are the number density for free electrons, atoms, and ions, respectively, i.e., the so-called plasma components. We see that within the LRT framework, the plasma components and MTCSs are required for the transport coefficient calculations. In the calculations, the MTCS for electron-atom scattering is calculated using partial wave decomposition, the MTCSs for electron-electron and electron-ion scatterings are calculated using the Born approximation (BA), and the plasma components are determined using SFVT.

2. *Potential models*

As is well known, the MTCS calculations depend strongly on the interaction potentials of the different scattering mechanisms. Therefore, appropriate potential models are vital for the MTCS calculations. We give a brief outline here, with additional detailed descriptions found elsewhere [31]. For electron scattering due to charged species in partially ionized plasmas, the dominant force is Coulombic interactions, which are screened by the other charged particles in the medium [15]. Here, we use the screened Coulomb potential (Debye potential) to describe the electron-ion and electron-electron interactions as

$$V_{SC}^{ei,ee}(r) = -\frac{Z_i}{r} e^{-r/r_0}, \tag{15}$$

where Z_i is the net charge of ions and electrons, $r_0 = r_D/(1 + v^2/v_{Th}^2)^{1/2}$ is the dynamic screening radius [32], v is the relative velocity of the colliding particles, v_{Th} is the thermal velocity, and $r_D = \sqrt{k_BT/4\pi e^2 n_e}$ is the Debye length. In this potential, the Debye length is replaced by the screening radius.

In electron-atom scattering, the dominant force is described as a dipole interaction, which is caused by the polarization of the atomic electron cloud as the scattering electron approaches the atom [15]. The polarization potential presented by Redmer *et al.* [33] was applied for electron-atom interactions in our previous work for Ar [26]. However, under warm dense conditions, the spatial distribution of electrons of an atom bound in a dense plasma environment is remarkably different from that of a free atom, which makes the description for electron-atom interactions more complex. For such complex interactions, a single polarization potential may not be sufficient as the plasma environmental effects may play an important role. To improve the descriptions for these interactions, an effective potential model in conjunction with the Muffin-tin model is applied here, which not only includes the static, exchange, and polarization interactions but also considers the plasma environmental effects [31]. Following the effective potential model, the interaction potential for scattering by atoms in a plasma is given by

$$V_{mt}(r) = \begin{cases} V_{s,mt}(r) + V_{ex}(r) + V_p(r) \text{ if } r < R_{mt} \\ V_{s,mt}(R_{mt}) + V_{ex}(R_{mt}) + V_p(r) \text{ if } r > R_{mt}, \end{cases} \tag{16}$$

where $V_{s,mt}$ is the electrostatic interaction energy with atoms in dense plasmas, V_{ex} and V_p are the exchange and polarization potentials, respectively, and R_{mt} is the Muffin-tin sphere radius. The Muffin-tin sphere radius is applied to consider the influence of the plasma environment, which is taken as the averaged interatomic radius as

$$R_{mt} = \left(\frac{3M}{4\pi N_A \rho}\right)^{1/3}, \tag{17}$$

where M is the atomic weight of the target atom. The electrostatic interaction energy with an atom at the origin of the coordinates $V_{s,mt}$ is approximated as

$$V_{s,mt}(r) = V_s(r) + V_s(2R_{mt} - r), \tag{18}$$

where $V_s(r)$ is the static Coulomb potential, which can be calculated by

$$\begin{aligned} V_s(r) &= -\frac{Z_a}{r} + \iiint \frac{\rho_e(\mathbf{r}')}{|\mathbf{r} - \mathbf{r}'|} d\tau \\ &= -\frac{Z_a}{r} + \frac{4\pi}{r}\int_0^r r'^2 \rho(r') dr' + 4\pi \int_r^\infty r' \rho(r') dr', \end{aligned} \tag{19}$$

where Z_a is the atomic number of the target atom and $\rho_e(r) = \sum_i \phi_i(r)\phi_i{}^*(r)$ is the bound electron density. Here, we use

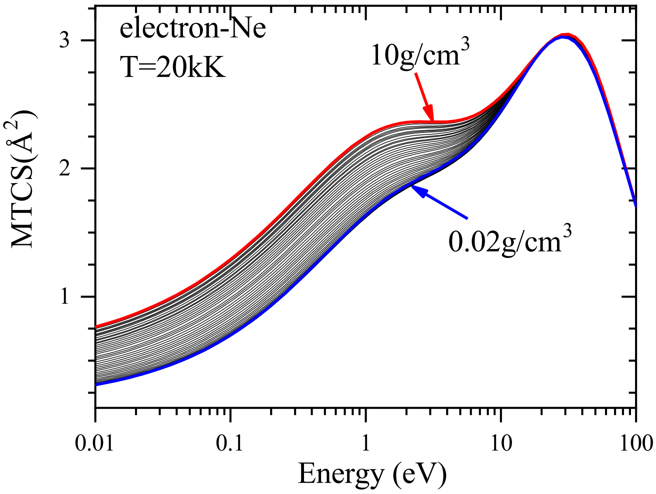

FIG. 1. The MTCS of elastic electron scattering by neon atoms as a function of the scattering energy in different plasma densities and a temperature of 20 kK.

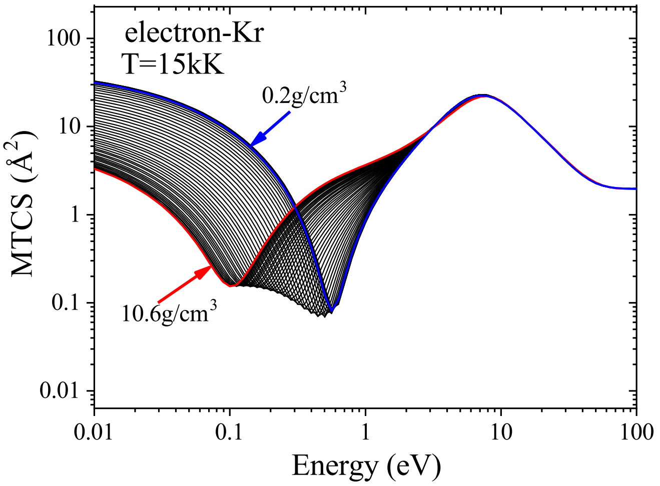

FIG. 2. The calculated MTCS of elastic scattering of electrons from Kr as a function of scattering energy in different plasma densities and a temperature of 15 kK.

the analytic Roothaan-Hartree-Fock atomic wave functions, $\phi_i(r)$, which was derived by Bunge and Barrientos [34].

The polarization potential $V_p(r)$ was calculated using the formula

$$V_p(r) = -\frac{\alpha_p}{2\left(r^2+r_a^2\right)^2}\left(1+\frac{r}{r_D}\right)^2 e^{-2r/r_D}, \tag{20}$$

where $\alpha_p = 3.956 \times 10^{-25}$ and 2.4844×10^{-24} cm^3 are the dipolar polarizabilities for Ne and Kr, respectively, and $r_a = (\alpha_p/2Z_a^{1/3})^{1/4}$ is a parameter related to the atom species. The exchange potential $V_{ex}(r)$ was calculated using the Hara local exchange approximation [35],

$$V_{ex}(r) = -\frac{2}{\pi}K_F\left[\frac{1}{2}+\frac{1-\eta^2}{4\eta}+\ln\left|\frac{1+\eta}{1-\eta}\right|\right], \tag{21}$$

where $\eta(r) = [\kappa_F^2(r)+2I+E_e]^{1/2}/\kappa_F(r)$, $\kappa_F(r) = [3\pi^2\rho_e(r)]^{1/3}$, E_e is the collision energy, and I is the first ionization potential.

III. RESULTS AND DISCUSSION

A. MTCS for electron-atom scattering under warm dense environments

As described in Sec. II B 2, under warm dense conditions, the effects of the plasma environment may play an important role in the MTCS of electron-atom scattering. To evaluate these effects, we calculate the MTCSs for electron-Ne and electron-Kr scattering over a wide density range as functions of the scattering energy, as shown in Figs. 1 and 2. Figure 1 shows the MTCS for electron-Ne scattering in a density range of $\rho = 0.02$–10 g/cm^3 at a constant temperature of $T = 20$ kK. It is seen that for electron-Ne scattering, the influence of the plasma density is significant at low scattering energies (<10 eV), but is nearly constant for higher energy scattering (>10 eV). This means that for electron-Ne scattering, the effects of the plasma density on the MTCS should be considered at low scattering energies and can be ignored at higher scattering energies. Figure 2 shows the MTCS for electron-Kr scattering in a density range $\rho = 0.2$–10.6 g/cm^3 at a constant temperature of $T = 15$ kK. For electron-Kr scattering, the significant influence from the plasma density is also observed at low scattering energies (<3 eV). This suggests that for electron-Kr scattering, the plasma density effect on the MTCS should also be considered at low scattering energies. Moreover, a density-dependent Ramsauer-Townsend minimum is found for electron-Kr scattering. The Ramsauer-Townsend minimum shifts towards lower scattering energies with an increasing density, and the MTCS decreases (increases) for densities below (above) the Ramsauer-Townsend minimum.

B. Transport properties under warm dense conditions

It is well known that the calculated conductivity of warm dense matter is strongly dependent on the accuracy of the MTCS and plasma component calculations. For warm dense Ne and Kr, the accuracy of the component calculations using the SFVT was validated by comparing the EOSs between the calculations and the shock compression experimental measurements [24,25,36]. Therefore, the key to test the adaptability of the model lies in the MTCS. We know the MTCS calculations are strongly related to the interaction potential model, which can be indirectly validated through comparisons of the conductivities between calculations and experiments after the plasma component accuracy is confirmed. Figure 3 shows the calculated electrical conductivities versus shock temperature for liquid Kr along its Hugoniot along with the available shock compression experimental results for liquid Kr [12] at pressures up to 90 GPa, temperatures up to 27 kK, and densities up to 7 g/cm^3, which provides a test benchmark for the adaptability of the model over a wide range of parameters. We see that the proposed SFVT + LRT model can nearly reproduce the experimental results, showing that the potential model is feasible to describe the MTCS of warm dense Kr at high densities. Moreover, the electrical conductivity calculated using only the polarization potential is also shown in Fig. 3 (labeled pol. potential) for comparison. It

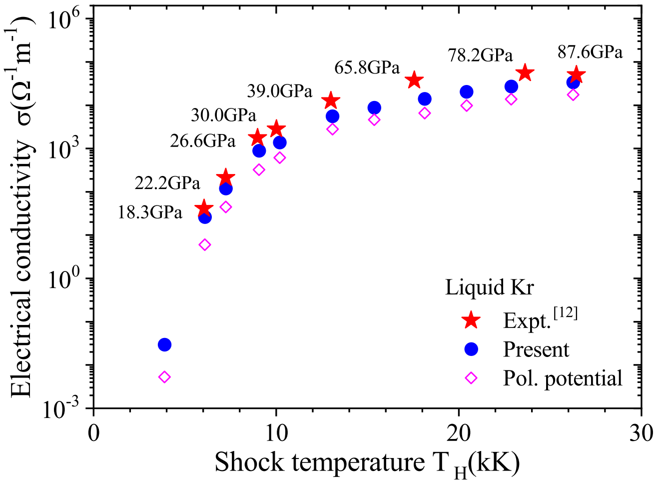

FIG. 3. Electrical conductivity vs shock temperature and shock pressure of liquid Kr along the principal Hugoniot curve.

is noted that the same plasma component, which is given in the SFVT, is used in the polarization potential electrical conductivity calculation. Comparing the results of the polarization potential shows that the calculated conductivities using the effective potential in the proposed model have a better agreement with the experiments. This shows that the effective potential model can provide an improved description for both electron-atom scattering and the conductivity of warm dense Kr. Figures 4(a)–4(d) show the calculated conductivity of dense Kr as a function of density over a wide range of densities and temperatures along with the available theoretical results from COMPTRA04 [37], Rosmej *et al.* [38], and Fortov *et al.* [39], which provides a comparison between the different models.

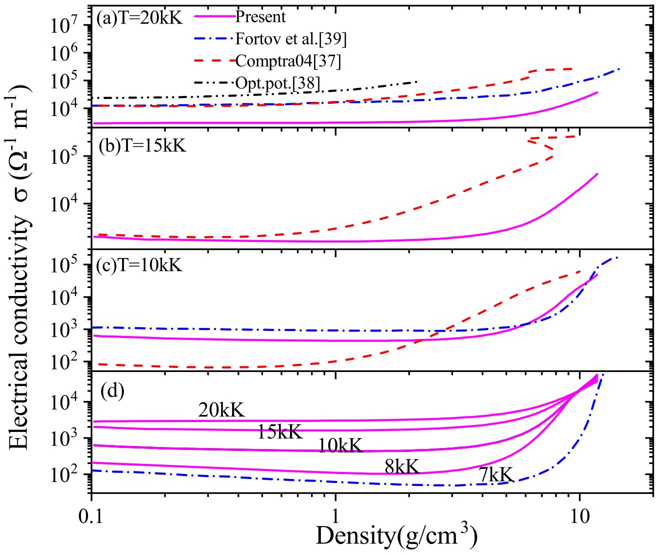

FIG. 4. Comparison of electrical conductivity vs density for warm dense Kr at different temperatures.

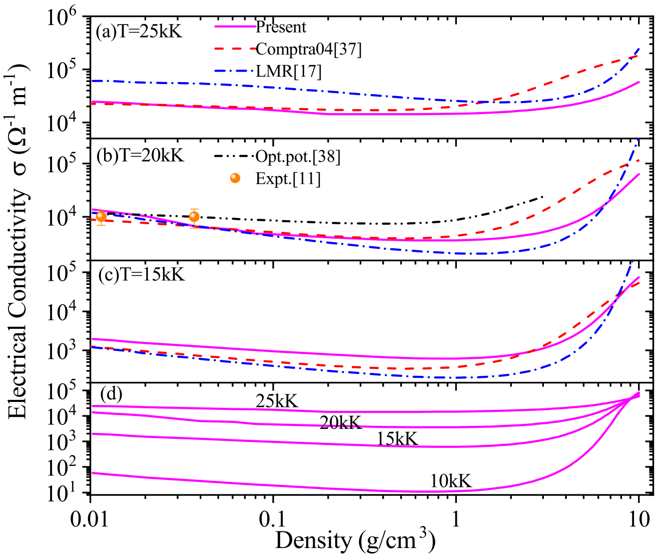

FIG. 5. Comparison of electrical conductivity vs density for warm dense Ne at different temperatures.

At low densities, our calculations are in agreement with those from COMPTRA04 at $T = 15$ kK and Fortov *et al.* at $T \sim 8$ kK. However, at high densities, apparent differences are seen between the different models. To further test the adaptability of the model as extended to lighter elements, the isothermal electrical conductivity of dense Ne was calculated over a wide region of densities and temperatures as a function of density, as shown in Figs. 5(a)–5(d). The results from COMPTRA04 [37], Rosmej *et al.* [38], LMR [17], and experiments [11] are also shown as a comparison. For Ne at $T = 20$ kK, all the calculations using different models, including the proposed model, are in good agreement with the experiments at low densities. The results show that the proposed model is feasible for warm dense Ne for at least low densities. At densities above 0.1 g/cm^3, there are obvious discrepancies among the various calculation models, which arise primarily from differences in the plasma components and interaction potentials used in the MTCS calculations. Moreover, for both Ne and Kr, similar behaviors with Ar [26] are observed. For example, at some temperature region, the electrical conductivities first decrease before rapidly increasing with the density, but they always increase with the density at higher temperatures. Another observation is that the electrical conductivities intercross with each other and are inverse at higher densities. These behaviors are related to the pressure ionization and nonmetal-metal transition (NMMT), which were illustrated in our previous work for Ar [26].

The thermopower characterizes the generation of an electric field as a response to temperature gradients and is important in the context of gas-filled voids that form under irradiation. Figures 6(a) and 6(b) present the calculated thermopower versus density for dense Ne and Kr plasmas at different temperatures, respectively, which illustrates the evolution of thermopower with both temperature and density. The results from COMPTRA04 [37] are also given as a comparison. There are differences between our calculations and the results from COMPTRA04. For Ne, our calculations indicate that the thermopower first increases rapidly up to a maximum from negative to positive with density at different temperatures before decreasing for our considered range, as seen in Fig. 6(a).

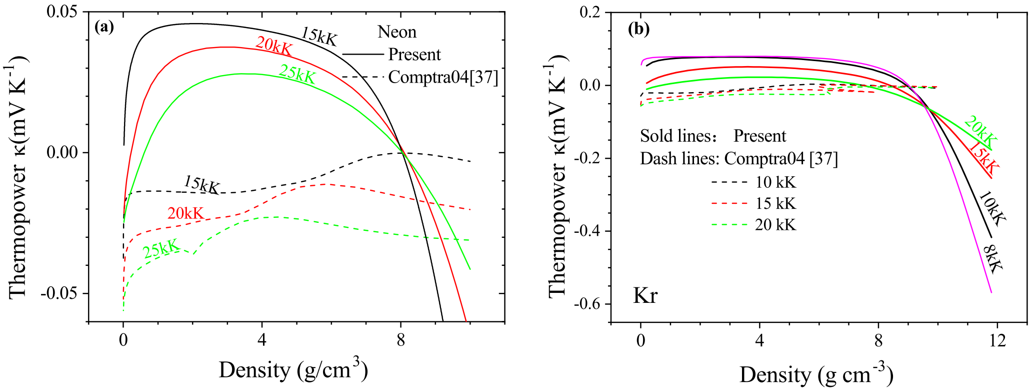

FIG. 6. Comparison of thermopower vs density with the COMPTRA04 for warm dense Ne and Kr at different temperatures.

These decreases are slow for the initial phase. However, when the density further increases to ∼6 g/cm^3, the decreases grow rapidly at a rate that is faster for lower temperatures. When at approximately 8 g/cm^3, the thermopower becomes negative and a “reversal” occurs, i.e., the thermopower of the lower temperature has smaller values than at higher temperatures. For Kr, similar behavior is observed, but the thermopower reversal occurs at an even higher density of ∼9.5 g/cm^3, as seen in Fig. 6(b). Compared with our calculations, the thermopower data given from COMPTRA04 are always negative and the evolution of the thermopower with temperature and density shows different characteristics.

Thermal conductivity is also a key parameter for the transport coefficients. At high temperatures and pressures, it is relatively difficult to produce theoretical results that are consistent with experiments. Some questions concerning theoretical descriptions and interpretations of the measurements data are still open. Figures 7(a) and 7(b) present the calculated thermal conductivity versus density for dense Ne and Kr plasmas at different temperatures, respectively. For warm dense Ne and Kr, there is no available experimental data of thermal conductivity. Therefore, we compare our calculations with the existing thermal conductivity data given by COMPTRA04 [37]. Figure 7(a) compares the thermal conductivity for dense Ne. Our calculations show a similar evolution tendency with the COMPTRA04 results in the considered range, but are only consistent at the lower temperature of $T = 15$ kK. There are discrepancies between the curves at higher temperatures, which become larger with temperature and density, with our results being smaller than the COMPTRA04. Figure 7(b) compares the thermal conductivity for dense Kr with notable deviations present. In particular, at densities from 4 to 6 g/cm^3 and temperatures from 15 to 20 kK, our calculations show different evolution tendencies than COMPTRA04 in the considered range. The differences arise primarily from the discrepancies in the plasma components and interaction potentials between the approaches. Moreover, the COMPTRA04 results show an instability region at temperatures of $T = 15$ and 20 kK, which did not occur in our calculations. These instabilities are due primarily to the atomic components having loops in the curves for COMPTRA04 (see Fig. 10 in Ref. [23]).

C. Plasma phase transition

The plasma phase transition (PPT) concept was introduced by Landau and Zeldovich in 1943 [40], and several researchers have since investigated phase transitions both experimentally [41] and theoretically [42,43]. However, PPT occurs in situations where both quantum and Coulomb effects are important, making the physical analysis more difficult. Here, the PPT of warm dense Kr is revisited from multiple perspectives regarding numerical simulation results for electrical conductivity and thermopower. Both the electrical conductivity and thermopower of warm dense Kr at densities from 9 to 10 g/cm^3 have an intercross point and show a reversal [see Figs. 4(d) and 6(b)]. As mentioned in our previous work for warm dense Ar, the intercross and reversal

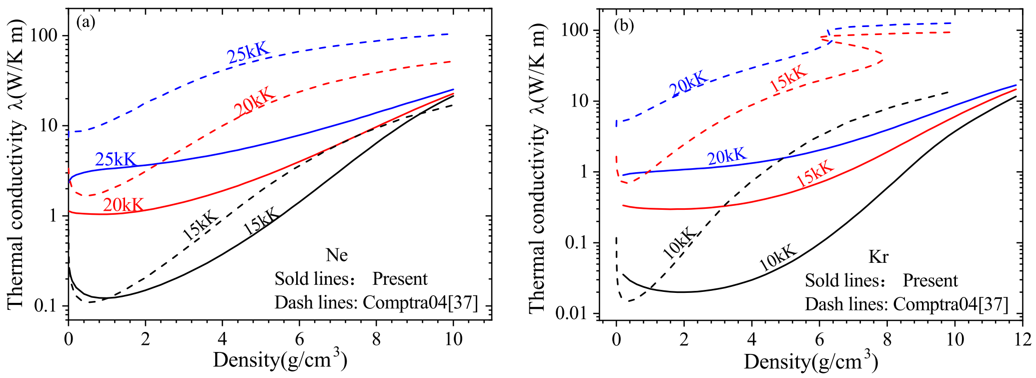

FIG. 7. Comparison of thermal conductivity vs density with COMPTRA04 [37] for warm dense Ne and Kr at different temperatures.

are related to the so-called NMMT [26]. Surprisingly, the density-temperature location for the NMMT, which is determined from the present intercross and reversal in the electrical conductivity and thermopower, is consistent with the PPT of warm dense Kr, which is given by the results of our previous EOS analysis [24]. This coincidence indicates that the NMMT found here for dense Kr may be connected to the PPT. A similar behavior was also found for dense Ne, as shown in Figs. 5(d) and 6(a).

IV. CONCLUSION AND OUTLOOK

An improved SFVT + LRT model is presented, in which an effective potential model in conjunction with the Muffin-tin model was applied to provide an improved description of electron-atom scattering. The model was used to calculate the transport coefficients, including the electrical conductivity, thermopower, and thermal conductivity, of warm dense Ne and Kr. The effective potential model allows not only including the static, exchange, and polarization interactions, but also considers the plasma environmental effects for electron-atom scattering. The improved SFVT + LRT is successfully extended to lighter and heavier elements (Ne and Kr) relative to previous results. The density effect on the MTCS for electron-atom scattering in plasmas is analyzed based on the effective potential model, and the resulting influence is significant at lower scattering energies but is different between the electron-Ne and electron-Kr scattering. For electron-Kr scattering, an important feature called the Ramsauer-Townsend minimum is observed, which depends on the relative densities. The "reversal" of the electrical conductivity and thermopower of warm dense Kr, which characterizes the so-called NMMT, was found at densities from 9 to 10 g/cm^3. The density-temperature location for the NMMT as determined from the reversal shows good consistency with the PPT, which was determined by the results of the EOS analysis in our previous work. This indicates that the NMMT found here for dense Kr may be connected with the PPT, which would require new theoretical and experimental data tests in the future. These observations are useful to better understand the transport properties of warm dense noble gases and may provide an important guide for future experimental designs and theoretical developments.

ACKNOWLEDGMENTS

This work is supported by the National Natural Science Foundation of China (Grants No. 11872057 and No. 11674292), the Foundation of National Key Laboratory of Shock Wave and Detonation Physics (Grants No. JCKYS2020212009, No. JCKYS2018212001, and No. 6142A0301020217), and the Science Challenge Project (Grant No. TZ2016001).

---

[1] M. D. Knudson and M. P. Desjarlais, Phys. Rev. Lett. **118**, 035501 (2017).

[2] K. R. Cochrane, R. W. Lemke, Z. Riford, and J. H. Carpenter, J. Appl. Phys. **119**, 105902 (2016).

[3] A. Fernandez-Pañella, M. Millot, D. E. Fratanduono, M. P. Desjarlais, S. Hamel, M. C. Marshall, D. J. Erskine, P. A. Sterne, S. Haan, T. R. Boehly, G. W. Collins, J. H. Eggert, and P. M. Celliers, Phys. Rev. Lett. **122**, 255702 (2019).

[4] R. Cauble, D. K. Bradley, P. M. Celliers, G. W. Collins, L. B. Da Silva, and S. J. Moon, Contrib. Plasma Phys. **41**, 239 (2001).

[5] L. Liu, Q.-F. Chen, Y.-J. Gu, W. Zhang, Z.-G. Li, C.-J. Li, Z.-Q. Wang, G.-J. Li, Y.-S. Lan, and X.-R. Chen, Appl. Phys. Lett. **115**, 231905 (2019).

[6] W. J. Nellis, S. T. Weir, and A. C. Mitchell, Phys. Rev. B **59**, 3434 (1999).

[7] W. J. Nellis, H. B. Radousky, D. C. Hamilton, A. C. Mitchell, N. C. Holmes, K. B. Christianson, and M. van Thiel, J. Chem. Phys. **94**, 2244 (1991).

[8] G. V. Boriskov, A. I. Bykov, R. I. Il'kaev, V. D. Selemir, G. V. Simakov, R. F. Trunin, V. D. Urlin, A. N. Shuikin, and W. J. Nellis, Phys. Rev. B **71**, 092104 (2005).

[9] N. S. Shilkin, S. V. Dudin, V. K. Gryaznov, V. B. Mintsev, and V. E. Fortov, J. Expt. Theor. Phys. **97**, 922 (2003).

[10] D. B. Sinars, M. A. Sweeney, C. S. Alexander, D. J. Ampleford, T. Ao, J. P. Apruzese, C. Aragon, D. J. Armstrong, K. N. Austin, T. J. Awe *et al.*, Phys. Plasmas **27**, 070501 (2020).

[11] Y. V. Ivanov, V. B. Mintsev, V. E. Fortov, and A. N. Dremin, J. Expt. Theor. Phys. **44**, 112 (1976).

[12] V. D. Glukhodedov, S. I. Kirshanov, T. S. Lebedeva, and M. A. Mochalov, J. Expt. Theor. Phys. **89**, 292 (1999).

[13] T. R. Mattsson, S. Root, A. E. Mattsson, L. Shulenburger, R. J. Magyar, and D. G. Flicker, Phys. Rev. B **90**, 184105 (2014).

[14] R. S. Mcwilliams, D. A. Dalton, Z. Konopkova, M. F. Mahmood, and A. F. Goncharov, Proc. Natl. Acad. Sci. USA **112**, 7925 (2015).

[15] J. R. Adams, H. Reinholz, R. Redmer, V. B. Mintsev, N. S. Shilkin, and V. K. Gryaznov, Phys. Rev. E **76**, 036405 (2007).

[16] S. Kuhlbrodt, R. Redmer, H. Reinholz, G. Ropke, B. Holst, V. B. Mintsev, V. K. Gryaznov, N. S. Shilkin, and V. E. Fortov, Contrib. Plasma Phys. **45**, 61 (2005).

[17] Z. J. Fu, Q. F. Chen, and X. Chen, Contrib. Plasma Phys. **52**, 251 (2012).

[18] M. P. Desjarlais, C. R. Scullard, L. X. Benedict, H. D. Whitley, and R. Redmer, Phys. Rev. E **95**, 033203 (2017).

[19] M. P. Desjarlais, Contrib. Plasma Phys. **41**, 267 (2001).

[20] W. Zhang, Z. Li, Z. Fu, J. Dai, Q. Chen, and L. Cai, Sci. Rep. **7**, 41885 (2017).

[21] B. Holst, M. French, and R. Redmer, Phys. Rev. B **83**, 235120 (2011).

[22] V. K. Gryaznov, I. Iosilevskiy, V. E. Fortov, A. N. Starostin, V. K. Roerich, V. A. Baturin, and S. V. Ayukov, Contrib. Plasma Phys. **53**, 392 (2013).

[23] S. Kuhlbrodt, B. Holst, and R. Redmer, Contrib. Plasma Phys. **45**, 73 (2005).

[24] Q. F. Chen, J. Zheng, Y. J. Gu, and Z. G. Li, Phys. Plasmas **22**, 122706 (2015).

[25] J. Tang, Y. J. Gu, Q. F. Chen, Z. G. Li, J. Zheng, C. J. Li, and J. T. Li, Phys. Rev. B **97**, 140101(R) (2018).

[26] W. L. Quan, Q. F. Chen, Z. J. Fu, X. W. Sun, J. Zheng, and Y. J. Gu, Phys. Rev. E **91**, 023106 (2015).

[27] H. Reinholz, R. Redmer, and S. Nagel, Phys. Rev. E **52**, 5368 (1995).

[28] R. Redmer, Phys. Rev. E **59**, 1073 (1999).

[29] S. Kuhlbrodt and R. Redmer, Phys. Rev. E **62**, 7191 (2000).

[30] D. N. Zubarev, *Nonequilibrium Statistical Thermodynamics* (NY Consultants Bureau, New York, 1974).

[31] F. Salvat, A. Jablonski, and C. J. Powell, Comput. Phys. Commun. **165**, 157 (2005).

[32] E. O. Shalenov, K. N. Dzhumagulova, and T. S. Ramazanov, Phys. Plasmas **24**, 012101 (2017).

[33] R. Redmer, T. Rother, K. Schmidt, W. D. Kraeft, and G. Ropke, Contrib. Plasma Phys. **28**, 41 (1988).

[34] C. F. Bunge, J. A. Barrientos, and A. V. Bunge, Atom. Data Nucl. Data Tab. **53**, 113 (1993).

[35] S. Hara, J. Phys. Soc. Jpn. **22**, 710 (1967).

[36] Z.-Q. Wang, Z.-G. Li, Y.-F. Wang, L. Liu, Y.-J. Gu, Q.-F. Chen, and X.-R. Chen, Phys. Rev. E **100**, 033214 (2019).

[37] See http://web.physik.uni-rostock.de/statphys/pages/comptra/ for the transport coefficient of noble gas.

[38] S. Rosmej, H. Reinholz, and G. Ropke, Phys. Rev. E **95**, 063208 (2017).

[39] V. E. Fortov, V. Y. Ternovoi, M. V. Zhernokletov, M. A. Mochalov, A. L. Mikhailov, A. S. Filimonov, A. A. Pyalling, V. B. Mintsev, V. K. Gryaznov, and I. L. Iosilevskii, J. Expt. Theor. Phys. **97**, 259 (2003).

[40] Y. B. Zeldovich and L. D. Landau, Zh. Eksp. Teor. Fiz **14**, 32 (1944).

[41] V. E. Fortov, R. I. Ilkaev, V. A. Arinin, V. V. Burtzev, V. A. Golubev, I. L. Iosilevskiy, V. V. Khrustalev, A. L. Mikhailov, M. A. Mochalov, V. Y. Ternovoi, and M. V. Zhernokletov, Phys. Rev. Lett. **99**, 185001 (2007).

[42] D. Saumon and G. Chabrier, Phys. Rev. Lett. **62**, 2397 (1989).

[43] M. A. Morales, C. Pierleoni, E. Schwegler, and D. M. Ceperley, Proc. Natl. Acad. Sci. USA **107**, 12799 (2010).